NOVEL MEDICAL WIRED PALPATION DEVICE: A VALIDATION STUDY OF MATERIAL PROPERTIES

X. Wang[1], C. Di Natali[2], M. Beccani[2], M. Kern[1], P.Valdastri[2], and M. Rentschler[1]
[1]University of Colorado, Boulder, CO, UNITED STATES
[2]Vanderbilt University, Nashville, TN, UNITED STATES

ABSTRACT

The lack of haptic feedback during Minimally Invasive Surgery (MIS) can be potentially dangerous, and has been a factor in preventing a wider application of MIS. A Wired Palpation Device (WPD), which is designed to provide the surgeon with soft tissue viscoelasticity information during MIS, can be an appealing solution to this challenge. As a novel device, the validation of its functionality is critical before being put into actual usage. In this paper, a procedure assessing the effectiveness of the WPD in characterizing soft tissue material properties was introduced. Strain creep indentation tests were performed using the WPD method on four different synthetic tissue samples, followed by standard stress relaxation indentation tests on the same samples. The results showed that the WPD was reliable in characterizing the long-term material response when compared to the traditional method (an average of 5.21% difference), but may still need improvement in its capability of capturing short-term transient soft tissue response.

INTRODUCTION

Today laparoscopic procedures are a widespread clinical practice where surgical instruments are inserted into the abdominal cavity through small incisions. However, the lack of nonvisible haptic feedback during minimally invasive surgery (MIS) has led to active research to mitigate this roadblock [1]. So far a significant number of MIS devices have been developed to restore the kinesthetic force and tactile feedback for the surgeon and acquire *in vivo* data for tissue modeling and simulation [2–5]. These devices generally rely on force and/or tactile sensors and are developed to work on soft complex tissues. Evidence showing that basic elastic models are only a rough approximation of the actual soft tissues have been reported by researchers for decades [6], [7]. Due to the strain-rate dependency of the soft tissue properties, viscosity is often observed during mechanical tests on these materials [8–10]. As a result, a viscoelastic model that combines elastic and viscous responses of the soft tissue has become a popular choice for tissue mechanics modeling. However, to the authors' knowledge, no existing palpation devices have taken this viscoelasticity into consideration while assessing the tissue properties through palpation [2], [3], [5], [11], [12]. Furthermore, all current palpation devices require a dedicated access port, thus limiting adoption by surgeons.

The proposed approach consists of a Wired Palpation Device (WPD) that can determine soft tissue viscoelastic properties by performing an *in vivo* creep test without any rigid connections to an external platform. The WPD is a soft-tethered magnetic device that can be deployed through a standard surgical trocar and operated to perform tissue palpation without taking up port space, as magnetic instrumentation described in [13–15].

Mechanical characterization of viscoelastic materials requires measurement of material response time-dependency. Two of the most common testing techniques to measure viscoelasticity are strain creep [16–18] and stress relaxation tests [19], [20]. The strain creep test applies a step change of stress to the material and maintains this stress over a given amount of time, while the change in tissue strain is measured with time. The stress relaxation test instead holds a fixed deformation while the change in stress is measured with time.

Feasibility of performing wireless palpation to quantify an elastic material response was demonstrated in [21] with a tetherless version of the WPD. The device proposed in this work was designed to perform at least one of the two fundamental viscoelastic testing methods above. With a proper setup, a strain creep test can be conducted using the WPD. In this paper, with the purpose of validating the effectiveness of the WPD in characterizing the viscoelasticity of soft tissue, four viscoelastic synthetic tissue samples with undetermined material properties went through strain creep indentation tests using the WPD. Later, the same four samples were again tested using widely accepted stress relaxation methods on a classical uniaxial MTS device. The comparison results between the two approaches presents a quantitative assessment of the WPD.

EXPERIMENTAL CONFIGURATIONS

MTS Indentation Approach

Traditional stress relaxation indentation tests were performed with a MTS Insight 2 Electromechanical Testing Systems (MTS System Corporation, MN). A load cell (MTS System Corporation, MN, PN LCCA-118-75) with a maximum capacity of 2 N and resolution of 0.001 N was used to measure the load, and all the data were collected and analyzed later with a customized program developed in MATLAB (MathWorks, MA). The MTS testing system was equipped with an axisymmetric, flat-ended cylindrical indentation tip of 14 mm diameter.

The samples were fixed to the supporting flat plate with double-sided tape, and were at rest under this constraint for 15 minutes before the indentation test. Prior to each indentation, the tip was manually controlled to move towards the top surface of the test material, until a clearance of about 1 mm was reached between the tip and the tissue surface. Then the movement of the tip was controlled by a customized testing algorithm to move at a velocity of 0.1 mm/s to establish an initial contact between the tip and the test material. The initial contact was considered formed when the load cell detected a load change of 0.001 N (the resolution of the load cell).

Once in initial contact, the control algorithm then drove the tip to indent a given depth (Specific values listed in Table 1) into the test material at a relatively high velocity (V

= 1 mm/s), to better simulate the theoretical step change of the indentation depth without causing dramatic vibration in the sample. After reaching the prescribed depth, the position of the indentation tip was fixed at this value for a given amount of time (t = 300 s). The relaxation time here was chosen to be 300 s, so that the test material response can reach a relatively stable state which gives information regarding long-term viscoelastic properties that facilitates the theoretical analysis. During the relaxation process, the load cell and software measured and recorded the load and time simultaneously at 100 Hz.

After each relaxation process was complete, the indentation tip was automatically moved back to its initial position where was no visual contact between the tip and the test material. The system stayed at this configuration for another 150 s, allowing the test material to stabilize before another trial was conducted following the procedure above.

Wired Palpation Device (WPD) Approach

The complete mechatronic system used to assess the Wired Palpation Device (WPD) is represented in Figure. 1 (left) and it consisted of the WPD, the robotic manipulator, central control unit and synthetic tissue sample being tested.

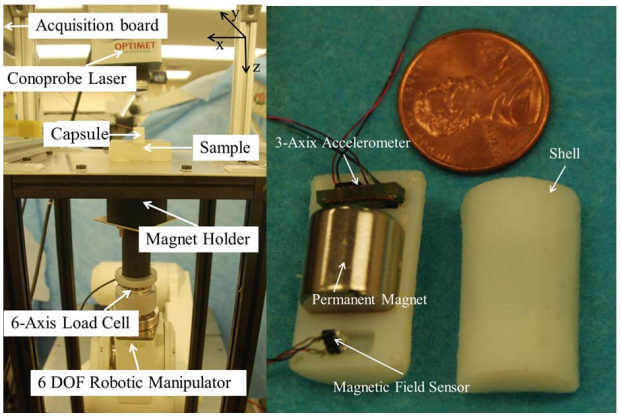

Figure. 1: Left: Overview of the complete WPD for vertical indentation. The conoprobe is used for indentation depth validation. Right: The detailed configuration of the WPD capsule.

The WPD capsule includes an embedded a permanent magnet and a sensing module inside a cylindrical shell (Figure. 1, right). An off-the-shelf cylindrical NdFeB permanent magnet (K&J Magnetics, Inc., USA), with 11 mm in diameter, 11 mm in height and N52 axial magnetization (magnetic remanence of 1.48 T) was used. The sensing module consisted of a Hall Effect sensor (CYP15A, Chen-Yang Technologies GmbH & Co. KG, Germany) to measure the Z component of the magnetic field, B, a tri-axial accelerometer used as inclinometer (LIS331AL, STMicroelectronics, Switzerland) - to verify that the capsule motion during the creep test was limited to the Z direction. An analog signal conditioning stage connected to the Hall effect sensor output allowed to cancel out the offset due to the onboard permanent magnet (*i.e.*, 98 mT), to apply a low-pass filter (cut-off frequency of 30 Hz), and to amplify by 33 the magnetic field signals, resulting in a resolution of 0.1 mT and a sensing range of ±120 mT. The angular resolution for the accelerometer was 0.3 degrees. All of the components were integrated inside a cylindrical plastic shell fabricated by rapid prototyping (OBJECT 30, Object Geometries Ltd, USA) and was 14 mm in diameter and 27.5 mm in height with a total weight of 12 g.

Concerning the robotic manipulator represented in Figure. 1, an off-the-shelf cylindrical NdFeB permanent magnet (5 cm in diameter and 5 cm in height), with N52 axial magnetization (magnetic remanence of 1.48 T), was adopted. The magnet was embedded in a plastic holder connected to a 6-axis load cell (MINI45, ATI Industrial Automation, Inc., USA), having a resolution of 65 mN for the Z component of the force. The magnet-load cell assembly was mounted at the end effector of a six degrees of freedom industrial robot (RV6SDL, Mitsubishi Corp., Japan), presenting a motion resolution of 1µm in each direction.

The central control unit consisted of two dedicated acquisition boards (NI USB 6211 and NI-PCI 6224, National Instruments, USA) to acquire the data coming from the capsule and the load cell, respectively. A Windows 7, 32-bit operating system, merged the data with the manipulator position. The data acquired from the load cell and the sensing module were processed in two parallel threads at a sample frequency of 1 kHz, while the central control unit performed a loop at 50 Hz implementing the closed-loop control to perform the creep test.

All of the creep trials were performed with the synthetic tissue samples placed on a 2 mm thick rigid support. Data from the accelerometer were used to confirm that the capsule motion was always occurring normal to the sample. An optical conoscopic holography sensor (Conoprobe, Optimet, USA) was adopted as reference measurement system to validate the creep test. The conoprobe was mounted so to point the laser spot on the upper circular surface of the capsule as in Figure. 1, left. The creep trial was based on the idea to keep constant the force exerted by the capsule on the tissue sample for the entire trial. The force applied by the WPD is generated by the interaction of the onboard and robotic manipulator magnets. Considering that the magnetic force is a function of the relative orientation and position of both magnets [22], the magnetic coupling can be fully characterized along the Z direction by the sensing module. The magnetic field closed-loop control system was designed to regulate the motion of the robotic manipulator to maintain a specified distance to the capsule within the range of 5 cm between the external and the internal magnet. The creep test started from a penetration preload phase of 0.5 mm of the capsule in the tissue sample. Then the input step phase occurred, in which the external magnetic manipulator moved upwards along z direction covering about 5 cm in 2 sec. This provided the rise in magnetic force that led the capsule to penetrate the sample. This second phase is called transient phase and the capsule penetrated at the speed of 1 mm/s. It is worth mentioning that, differently from [21], here data were transmitted from the WPD over a cable connection due to the high data rate required to close the robotic control loop.

Sample Preparation

The four synthetic tissue samples were produced by combining two kinds of liquid plastic (PVC Regular Liquid Plastic and Super Soft Liquid Plastic - MF Manufacturing –USA) and two plasticizers (Plastic Softener and Plastic

Hardener - MF Manufacturing –USA). After mixing 140 g of liquid plastic with 35 g of plasticizer, the liquid was heated for 7 minutes, degassed, stirred gradually and then poured into a squared mold of 75 mm with 25 mm in height. With this fabrication technique, the four tissue samples showed limited variability in both the side dimensions (72.86 ±0.80 mm) and height (23.02 ±0.72 mm). The center point from the top surface was selected to be the sampling point for indentation. These parameters are listed in Table 1.

Table 1: Sample Dimensions and Test Parameters

Sample	Length (mm)	Thickness (mm)	Indentation Depth[a] (mm)	Indentation Load[b] (N)
1	72.83	22.30	1.37	2.16
2	73.09	23.70	2.07	1.99
3	73.10	22.60	2.45	1.03
4	72.93	23.70	2.15	1.92

a. The indentation depth is used for MTS only.
b. The indentation load is used for WPD only.

THEORETICAL DERIVATION

Theoretical equations relating the collected experimental indentation data to the desired viscoelastic material properties is needed for data analysis. In this section, such theoretical equations are introduced for both the stress relaxation and strain creep tests.

Stress Relaxation Equation

For a viscoelastic stress relaxation problem, the Wiechert model is widely accepted due to its capability of characterizing accurate viscoelastic response [3], [23], [24]. As shown in Figure. 2, it consists of one linear spring and several spring-dashpot units (Maxwell unit).

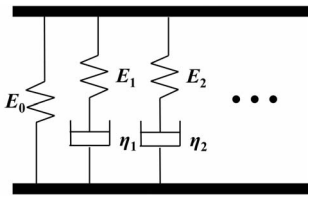

Figure. 2: The Wiechert model for viscoelastic material. The model is created by connecting one elastic spring and unspecified number of Maxwell units in parallel. This form is mathematically convenient for stress relaxation problems.

In this model, E_0 is the linear spring modulus, and E_i is the modulus of the ith Maxwell unit. The viscosity of the dashpot in the ith Maxwell unit is defined as η_i, which is commonly used with E_i to produce the relaxation time, τ_i as

$$\tau_i = \frac{\eta_i}{E_i}. \tag{1}$$

For a stress relaxation indentation test modeled with a Wiechert model, the desired equation relating the load, $F(t)$, to the model parameters (E_i and τ_i) can be derived as [25]

$$F(t) = \frac{8Rd}{3}\left(E_0 + \sum_{i=1}^{n} E_i e^{-t/\tau_i}\right) \quad n=1, 2, 3..., \tag{2}$$

where R is the radius of the indentation tip, d is the indentation depth, and n is the number of Maxwell units in the model. In this equation, the sample is assumed to be incompressible giving a Poisson's ratio of 0.5, which is reasonable assumption since most such synthetic materials can be considered incompressible under normal loads.

Strain Creep Equation

The strain creep test is different from the stress relaxation test in that the indentation load, instead of the depth, is now a constant value during the test. To avoid unduly mathematical complexities [26], a congruent form of the Wiechert model is introduced here for the creep analysis, as shown in Figure. 3.

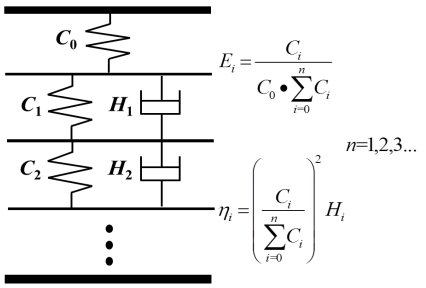

Figure. 3: A congruent form of the Wiechert model (Figure. 2), with n *Kelvin units connected in series. For a strain creep associated problem, this model has the advantage of mathematical simplicity.*

In this model, the Maxwell unit is replaced by a basic parallel spring-dashpot combination unit (Kelvin unit), and these units are connected to the linear spring in series. The compliance term, C_i, which is the inversion of the modulus, is now used to facilitate the mathematical manipulation. The dashpot viscosity in this model is defined as H_i. Also, although different in model configuration, the terms between the two models (Figure. 2 and Figure. 3) are interchangeable with the conversion equations shown to the right of Figure. 3. The desired equation for modeling strain creep results with the congruent model is derived by following the viscoelastic correspondent method [27].

The corresponding elastic problem of the strain creep viscoelastic problem studied here can be described as an indentation problem between a flat-ended rigid cylindrical tip and a pure elastic test material. The analytical equation relating the total indentation load, F, to the indentation depth, d, on a half-space (infinite large) elastic test material, has already been determined [28] as

$$d = \frac{3F}{8ER} = \frac{3F}{8R}C, \tag{3}$$

where R is the radius of the indentation tip, E is the elastic modulus and, and C is the compliance of the material and is defined as $1/E$. In this problem, the test material (synthetic tissue) is also assumed to be incompressible.

Applying the Laplace transformation to (3) and denoting the transformed functions with an overline, the depth, d, can be expressed in the space-domain as

$$\bar{d}(s) = \frac{3\bar{F}(s)\bar{C}(s)}{8\bar{R}(s)} = \frac{3}{8R}\bar{F}(s)\bar{C}(s) \tag{4}$$

where s is the basic variable in space-domain after the transform. Since a step change of the indentation load is assumed here, the indentation load, F, is actually expressed as

$$F(t) = F \bullet u(t), = \begin{cases} 0, & t < 0 \\ F, & t \geq 0. \end{cases} \quad (5)$$

where F is the constant indentation load value and $u(t)$ is a Heaviside function defined. Therefore, the expression of $F(t)$ in the space domain is

$$\bar{F}(s) = \frac{F}{s}. \quad (6)$$

Substituting (6) and replacing the elastic term $\bar{C}(s)$ with its viscoelastic analog, $\bar{C}_v(s)$, (4) becomes

$$\bar{d}(s) = \frac{3F}{8R}\frac{\bar{C}_v(s)}{s}. \quad (7)$$

Applying inverse Laplace transformation to (7), the equation expressing the indentation depth, d, in terms of viscoelastic model parameters in the time domain is derived as

$$d(t) = \frac{3F}{8R}C_v(t), \quad (8)$$

where $C_v(t)$ is the expression of $\bar{C}_v(s)/s$ in the time domain. The term $\bar{C}_v(s)$ will take different forms when different viscoelastic models are used. The inverse Laplace Transformation of this term can be awkward if an improper model is chosen. This is the primary reason for not using the Wiechert model for modeling creep test results.

For a model with n Kelvin units, term $\bar{C}_v(s)$ in (7) is expressed as [27]

$$\bar{C}_v(s) = C_0 + \sum_{i=1}^{n}\frac{1}{1/C_i + sH_i}. \quad (9)$$

Substituting (9) into (7) and applying inverse Laplace transformation to (7), the correspondent (8) for this model is derived as

$$d(t) = \frac{3F}{8R}(C_0 + \sum_{i=1}^{n}C_i - \sum_{i=1}^{n}C_i e^{-\frac{t}{C_i H_i}}), \quad n=1,2,3.... \quad (10)$$

RESULTS AND DISCUSSION

In this section, (2) and (10) are used to fit model parameters to the strain creep results collected using the WPD and the stress relaxation data gathered using the MTS were fitted to the derived theoretical equations. These model parameters are then quantitatively compared.

Indentation Test Results

The creep test results using the WPD consisted of two phases, *i.e.* the transient and the regime phase. During the transient phase, the manipulator moved 4 cm towards the rigid support in about 2 s, enabling the WPD to penetrate the tissue of about 10% of its thickness. Figure. 4 shows the manipulator position during the transient phase, highlighting a 2 mm overshoot and a settling time of 10 s.

During the regime phase, the typical indentation depth on tissue samples was in the range of 0.1 mm. Considering that the force needed to indent 10% of the sample thickness corresponds to a magnetic field value (0.1027 ±0.001 T), it was possible to obtain the linear control relationship between the robot manipulator motion and the magnetic field measured for the regime phase. Figure. 5 shows experimental data used to quantify this relationship, which is:

$$y = 230 \times x - 23. \quad (11)$$

where y is the manipulator position and x is the system input given by the measure of the magnetic field. Therefore for each variation of 1 mT in the input system the magnetic manipulator moves 0.23 mm. During the regime phase, thanks to the amplification and the high resolution of the magnetic feedback, a resolution of 0.0023 mm for the external magnetic manipulator control motion was achieved.

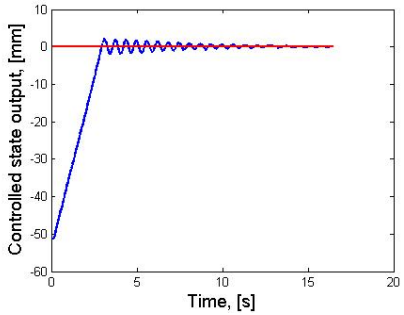

Figure. 4: Transient phase, this is the steep response of the robotic manipulator motion, which causes the WPD penetration in the sample.

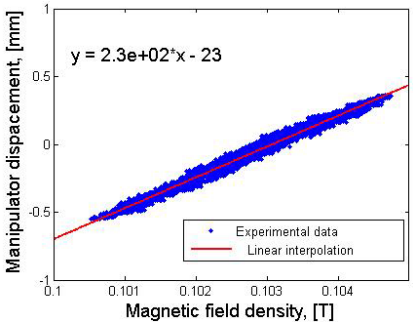

Figure. 5: Regime phase, linear relationship implemented on the robotic manipulator servo control.

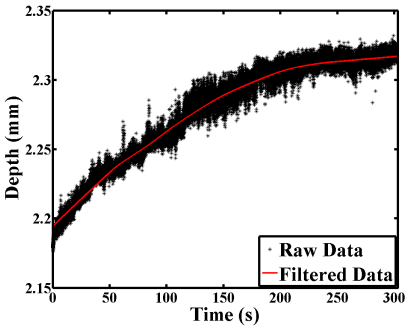

Figure.6: Indentation depth raw data from creep tests using WPD and the filtered data with moving average algorithm for sample 4, plotted against time.

One representative depth-time curve from the strain creep test raw data using the WPD on sample 4 is shown in Figure.6. The data was then filtered with a moving average algorithm before being fitted to (10).

For the stress relaxation test using the MTS, the collected data was used to create depth-time plots for analysis. One representative load-time plot on sample 4 is shown in Figure.7.

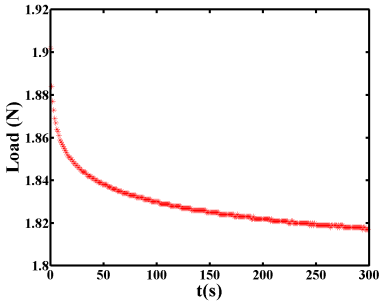

Figure.7: Load-time plot during a stress relaxation test for all three trials on Sample 4.

Curve Fitting Results

The Wiechert model is a general viscoelastic model with unspecified number of Maxwell units in its configuration. Here, models with up to three ($n \leq 3$) Maxwell or Kelvin units were used to fit the experimental data. The one unit model is a well-known basic viscoelastic model termed Standard Linear Solid (SLS) model. For convenience, the models with 2 and 3 units were are labeled Double Maxwell unit Wiechert (DMW) model and Triple Maxwell unit Wiechert (TMW) model, respectively.

As shown in Figure. 8, the filtered depth-time data curve from the WPD (shown in Figure. 6) was fitted with the SLS, DMW and TMW models using (10). These fitting processes gave the model parameters in terms of compliances (C_i) and viscosities (H_i), which can be expressed in terms of E_i and τ_i using Figure. 3. With MTS indentation test data the model parameter values for with all three models can be derived by fitting (2) to the stress relaxation data (an example is shown in Figure.9).

One finding emerges regarding a proper model selection for further analysis. For the creep tests using the WPD, the SLS model displayed the same level of accuracy (R^2 = 0.992) in data fitting as those with the higher order models, *i.e.* the DMW (R^2 = 0.995) and TMW (R^2 = 0.995) models. However, this is not the case for stress relaxation test. Observed from Figure.9, the SLS model behaves poorly in fitting the experimental data (R^2 = 0.754) while the DMW and TMW model still show decent match (an average R^2 = 0.991). Since additional units to the model bring more mathematical terms to the expression, the TMW model is more computationally expensive than the DMW model. As a result, the DMW model was chosen as the model for model parameter values comparison among the two approaches (Table 2), as it maintains a balance between model accuracy and mathematical simplicity.

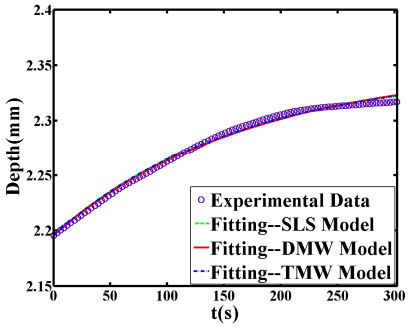

Figure. 8: The curve fittings using (10) for strain creep test results from the WPD on sample 4.

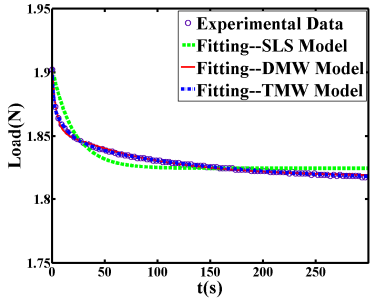

Figure.9: The curve fittings using (2) for stress relaxation test from the MTS on sample 4.

Table 2: DMW Model Parameter Values Derived From Both Test Approaches

Sample	Method	E_0 kPa	E_1 kPa	E_2 kPa	τ_1 (s)	τ_2 (s)	R^2
1	MTS	71.37	2.29	1.68	3.08	85.80	0.989
	WPD	74.19	2.39	3.77	16.91	397.00	0.997
2	MTS	46.82	1.00	0.82	3.32	88.83	0.989
	WPD	48.13	0.26	2.68	6.14	547.15	0.992
3	MTS	24.87	0.49	0.38	2.57	85.17	0.985
	WPD	23.49	0.22	1.61	28.05	506.76	0.921
4	MTS	45.35	1.16	0.97	3.65	87.95	0.991
	WPD	43.86	1.29	1.75	151.09	151.33	0.995

The derived model parameters from Table 2 were used to simulate a theoretical stress relaxation indentation test. The simulated test indented a 14 mm diameter tip to a constant indentation depth of 3 mm on an infinite large sample modeled by the DMW model. Substituting model parameter values into (2), the simulated load-time curves were created and shown in Figure. 10.

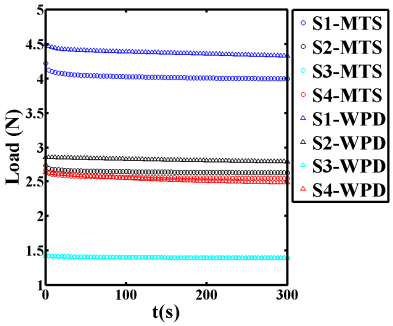

Figure. 10: The simulated stress relaxation responses of the four samples using both approaches. Curves with the same color were from the same material sample.

It is observed from Figure. 10 that both approaches successfully distinguished the four samples from each other. In terms of long-term effect, sample 1 has the highest stiffness while sample 3 being the softest. Sample 2 and sample 4 placed between sample 1 and 3, with sample 2 slightly harder than sample 4. This result can be treated as evidence proving the effectiveness of the WPD in determining long-term effects in the soft tissue.

However, if the short-term effect was analyzed, the WPD setup didn't work as well as the traditional testing method using the MTS (Figure.11). As shown in Figure.11, the performance of the WPD in capturing rapid changes in data at the very beginning is compromised due to the vibration in data itself. The filtering of raw data during the creep test caused the loss of these data at the beginning of the test.

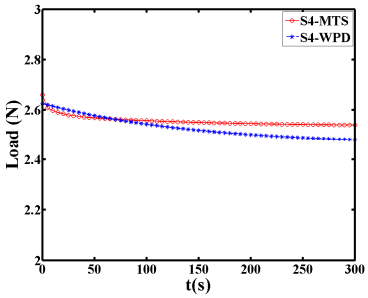

Figure.11: The simulated stress relaxation indentation test load-time curves using both approaches on sample 4.

CONCLUSION

The Wired Palpation Device (WPD) is a novel medical palpation device, and can be used to characterize the material properties of soft tissue modeled with viscoelastic material models. By comparing its testing results to standard stress relaxation test results, the reliability of the WPD in determining long-term soft tissue modulus is verified, with an average of 5.21% differences in reported long-term moduli (E_0) values between the two approaches.

However, the WPD still needs improvement before being used to characterize transient effect of the materials showing time-dependent properties. Several aspects are being studied to improve the system's transient performance, such as better hardware setup with more accurate magnetic sensor for load control, and improved data filtration process to capture transient data change.

REFERENCES

[1] P. Puangmali, K. Althoefer, L. D. Seneviratne, D. Murphy, and P. Dasgupta, "State-of-the-Art in Force and Tactile Sensing for Minimally Invasive Surgery," *IEEE Sensors Journal*, vol. 8, no. 4, pp. 371 –381, Apr. 2008.

[2] M. Ottensmeyer and J. Salisbury, "*In vivo* Data Acquisition Instrument for Solid Organ Mechanical Property Measurement," in *Medical Image Computing and Computer-Assisted Intervention – MICCAI 2001*, vol. 2208, W. Niessen and M. Viergever, Eds. Springer Berlin / Heidelberg, 2001, pp. 975–982.

[3] E. Samur, M. Sedef, C. Basdogan, L. Avtan, and O. Duzgun, "A robotic indenter for minimally invasive measurement and characterization of soft tissue response," *Medical Image Analysis*, vol. 11, no. 4, pp. 361–373, Aug. 2007.

[4] J. Rosen, J. D. Brown, S. De, M. Sinanan, and B. Hannaford, "Biomechanical Properties of Abdominal Organs *In vivo* and Postmortem Under Compression Loads," *J. Biomech. Eng.*, vol. 130, no. 2, pp. 021020–17, Apr. 2008.

[5] K. Lister, Z. Gao, and J. Desai, "Development of <i>In vivo</i> Constitutive Models for Liver: Application to Surgical Simulation," *Annals of Biomedical Engineering*, vol. 39, no. 3, pp. 1060–1073, 2011.

[6] K. Miller and K. Chinzei, "Constitutive modelling of brain tissue: Experiment and theory," *Journal of Biomechanics*, vol. 30, no. 11–12, pp. 1115–1121, November.

[7] K. Miller, "Constitutive model of brain tissue suitable for finite element analysis of surgical procedures," *Journal of Biomechanics*, vol. 32, no. 5, pp. 531–537, May 1999.

[8] K. Kumar, M. E. Andrews, V. Jayashankar, A. K. Mishra, and S. Suresh, "Measurement of Viscoelastic Properties of Polyacrylamide-Based Tissue-Mimicking Phantoms for Ultrasound Elastography Applications," *IEEE Transactions on Instrumentation and Measurement*, vol. 59, no. 5, pp. 1224–1232, May 2010.

[9] S. Marchesseau, T. Heimann, S. Chatelin, R. Willinger, and H. Delingette, "Fast porous visco-hyperelastic soft tissue model for surgery simulation: Application to liver surgery," *Progress in Biophysics and Molecular Biology*, vol. 103, no. 2–3, pp. 185–196, Dec. 2010.

[10] M. Sedef, E. Samur, and C. Basdogan, "Real-Time Finite-Element Simulation of Linear Viscoelastic Tissue Behavior Based on Experimental Data," *IEEE Computer Graphics and Applications*, vol. 26, no. 6, pp. 58–68, Dec. 2006.

[11] G. L. McCreery, A. L. Trejos, M. D. Naish, R. V. Patel, and R. A. Malthaner, "Feasibility of locating tumours in lung via kinaesthetic feedback," *The International Journal of Medical Robotics and Computer Assisted Surgery*, vol. 4, no. 1, pp. 58–68, 2008.

[12] J. C. Gwilliam, Z. Pezzementi, E. Jantho, A. M. Okamura, and S. Hsiao, "Human vs. robotic tactile sensing: Detecting lumps in soft tissue," in *2010 IEEE Haptics Symposium*, 2010, pp. 21 –28.

[13] M. Simi, G. Sardi, P. Valdastri, A. Menciassi, and P. Dario, "Magnetic Levitation camera robot for endoscopic surgery," in *2011 IEEE International Conference on Robotics and Automation (ICRA)*, 2011, pp. 5279 –5284.

[14] S. Park, R. A. Bergs, R. Eberhart, L. Baker, R. Fernandez, and J. A. Cadeddu, "Trocar-less Instrumentation for Laparoscopy," *Ann Surg*, vol. 245, no. 3, pp. 379–384, Mar. 2007.

[15] B. S. Terry, Z. C. Mills, J. A. Schoen, and M. E. Rentschler, "Single-port-access surgery with a novel magnet camera system," *IEEE Trans Biomed Eng*, vol. 59, no. 4, pp. 1187–1193, Apr. 2012.

[16] O. Starkova, G. C. Papanicolaou, A. G. Xepapadaki, and A. Aniskevich, "A method for determination of time- and temperature-dependences of stress threshold of linear–nonlinear viscoelastic transition: Energy-Based Approach," *Journal of Applied Polymer Science*, vol. 121, no. 4, pp. 2187–2192, Aug. 2011.

[17] E. D. Ryan, T. J. Herda, P. B. Costa, A. A. Walter, K. M. Hoge, J. R. Stout, and J. T. Cramer, "Viscoelastic creep in the human skeletal muscle–tendon unit," *Eur J Appl Physiol*, vol. 108, no. 1, pp. 207–211, Nov. 2009.

[18] J.-Y. Lim, H. C. Harrat, S. Choi, E. G. Nibaldi, E. M. Phillips, J. J. Widrick, and W. R. Frontera, "Relationship Bewteen Viscoelastic Stress Relaxation and Passive Stiffness in Single Muscle Fibers of Human Skeletal Muscles," *Medicine & Science in Sports & Exercise*, vol. 42, p. 378, May 2010.

[19] V. M. Punjabi, D. J. Bokor, M. H. Pelletier, and W. R. Walsh, "The Effect on Loop Elongation and Stress Relaxation During Longitudinal Loading of FiberWire in Shoulder Arthroscopic Knots," *Arthroscopy*, vol. 27, no. 6, pp. 750–754, Jun. 2011.

[20] M. Wathier and M. W. Grinstaff, "Synthesis and Creep-Recovery Behavior of a Neat Viscoelastic Polymeric Network Formed through Electrostatic Interactions," *Macromolecules*, vol. 43, no. 22, pp. 9529–9533, Nov. 2010.

[21] M. Beccani, C. Natali, M. Rentschler, and P. Valdastri, "Wireless Tissue Palpation: Proof of Concept for a Single Degree of Freedom," *IEEE International Conference on Robotics and Automation*, Karlsruhe, Germany, May, 2013.

[22] E. P. Furlani, *Permanent Magnet and Electromechanical Devices: Materials, Analysis, and Applications*. Academic Press, 2001.

[23] B. Ahn and J. Kim, "Measurement and characterization of soft tissue behavior with surface deformation and force response under large deformations," *Medical Image Analysis*, vol. 14, no. 2, pp. 138–148, Apr. 2010.

[24] B. B. Baran and C. Basdogan, "Force-Based Calibration of a Particle System for Realistic Simulation of Nonlinear and Viscoelastic Soft Tissue Behavior," in *Haptics: Generating and Perceiving Tangible Sensations*, vol. 6191, A. M. L. Kappers, J. B. F. Erp, W. M. Bergmann Tiest, and F. C. T. Helm, Eds. Berlin, Heidelberg: Springer Berlin Heidelberg, 2010, pp. 23–28.

[25] X. Wang, J. A. Schoen, and M. E. Rentschler, "A Comparison of Soft Tissue Compressive Viscoelastic Model Accuracy," *Journal of Mechanical Behavior of Biomedical Materials*, vol. 20, pp. 126-136, Apr. 2013.

[26] D. Roylance, "Engineering viscoelasticity," *Departament of Materials Science and Engineering Massachusetts Institute of Technology, Cambridge*, 2001.

[27] W. N. Findley, J. S. Lai, and K. Onaran, *Creep and relaxation of nonlinear viscoelastic materials: with an introduction to linear viscoelasticity*. Courier Dover Publications, 1989.

[28] A. C. Fischer-Cripps, *Introduction to contact mechanics*. Springer, 2000.

CONTACT

* Pietro Valdastri, e-mail: p.valdastri@vanderbilt.edu